Publication Year	2020
Acceptance in OA@INAF	2021-01-19T14:22:35Z
Title	The web of the Giant: spectroscopic confirmation of a Large Scale Structure around the z=6.31 quasar SDSS J1030+0524
Authors	Mignoli, M.; Gilli, R.; Decarli, R.; Vanzella, E.; Balmaverde, B.; et al.
DOI	10.1051/0004-6361/202039045
Handle	http://hdl.handle.net/20.500.12386/29850
Journal	ASTRONOMY & ASTROPHYSICS
Number	642

Astronomy & Astrophysics manuscript no. Letter_LBGs
September 3, 2020
©ESO 2020

Letter to the Editor

The web of the Giant: spectroscopic confirmation of a Large Scale Structure around the z=6.31 quasar SDSS J1030+0524

Marco Mignoli[1] ⋆, Roberto Gilli[1], Roberto Decarli[1], Eros Vanzella[1], Barbara Balmaverde[2], Nico Cappelluti[3], Letizia P. Cassarà[4], Andrea Comastri[1], Felice Cusano[1], Kazushi Iwasawa[5,6], Stefano Marchesi[1], Isabella Prandoni[7], Cristian Vignali[8,1], Fabio Vito[9], Giovanni Zamorani[1], Marco Chiaberge[10], and Colin Norman[10,11]

[1] INAF – Osservatorio di Astrofisica e Scienza delle Spazio di Bologna, OAS, via Gobetti 93/3, I-40129 Bologna, Italy
[2] INAF – Osservatorio Astrofisico di Torino, Via Osservatorio 20, I-10025 Pino Torinese, Italy
[3] Department of physics, University of Miami, Coral Gables, FL 33124, USA
[4] INAF – Istituto di Astrofisica Spaziale e Fisica Cosmica (IASF), Via A. Corti 12, 20133 Milano, Italy
[5] Institut de Ciències del Cosmos (ICCUB), Universitat de Barcelona (IEEC-UB), Martí i Franquès, 1, 08028 Barcelona, Spain
[6] ICREA, Pg. Lluís Companys 23, 08010 Barcelona, Spain
[7] INAF – Istituto di Radioastronomia, via Gobetti 101, I-40129 Bologna, Italy
[8] Dipartimento di Fisica e Astronomia, Università degli Studi di Bologna, Via Gobetti 93/2, I-40129 Bologna, Italy
[9] Scuola Normale Superiore, Piazza dei Cavalieri 7, I-56126 Pisa, Italy
[10] Space Telescope Science Institute, 3700 San Martin Dr., Baltimore, MD 21210, USA
[11] Johns Hopkins University, 3400 N. Charles Street, Baltimore, MD 21218, USA

Received / Accepted

ABSTRACT

We report on the spectroscopic confirmation of a large scale structure around the luminous, z=6.31 QSO SDSS J1030+0524, that is powered by a billion solar mass black hole. The structure is populated by at least six members, four Lyman Break Galaxies (LBGs) and two Lyman Alpha Emitters (LAEs). The four LBGs have been identified among a sample of 21 i-band dropouts with $z_{AB} < 25.5$ selected up to projected separations of 5 physical Mpc (15 arcmin) from the QSO. Their redshifts have been determined through up to 8hr-long multi-object spectroscopic observations at 8-10m class telescopes. The two LAEs have been identified in a 6hr VLT/MUSE observation centered on the QSO. The redshifts of the six galaxies cover the range 6.129-6.355. Assuming that peculiar velocities are negligible, this range corresponds to radial separations of ±5 physical Mpc from the QSO, that is comparable to the projected scale of the observed LBG distribution on the sky. We conservatively estimate that this structure is significant at $> 3.5\,\sigma$ level, and that the level of the galaxy overdensity is at least 1.5-2 within the large volume sampled (∼780 physical Mpc^3). The spectral properties of the six member galaxies (Lyα strength and UV luminosity) are similar to those of field galaxies at similar redshifts.
This is the first spectroscopic identification of a galaxy overdensity around a super-massive black hole in the first billion years of the Universe. Our finding lends support to the idea that the most distant and massive black holes form and grow within massive ($> 10^{12}\,M_\odot$) dark matter halos in large scale structures, and that the absence of earlier detections of such systems was likely due to observational limitations.

Key words. galaxies: high-redshift — quasars: general — quasars: super massive black holes: individuals: SDSS J1030+0524

arXiv:2009.00024v2 [astro-ph.GA] 2 Sep 2020

1. Introduction

The existence of Super-Massive Black Holes (SMBHs; with masses of 10^{8-10}M$_\odot$) powering luminous quasars at z∼6 and beyond is a severe challenge for extra-galactic astronomy. Theory strongly argues that these objects must have formed and grown within the most massive dark matter halos ($M_{\rm halo}$∼$10^{12-13}\,M_\odot$) in highly biased regions of the early Universe, where seed black holes may find suitable physical conditions to form and sufficiently large reservoirs of gas to grow (Sijacki et al. 2009; Barai et al. 2018; Wise et al. 2019). Within these environments, high accretion rates can be triggered and sustained by both frequent mergers of proto-galaxies and possibly by steady flows of cold gas from which the galaxies can form. Such early large scale structures (LSSs), whose cores would eventually evolve into local massive galaxy clusters, are expected to be traced by significant galaxy overdensities that may extend up to scales of ∼10 physical Mpc (pMpc) from the quasar (Overzier et al. 2009).

The actual number and physical properties of galaxies in early overdensities, however, heavily depend on the competing processes that promote or prevent galaxy assembly. The same is true for their spatial distribution. For instance, both supernovae explosions in these galaxies and the release of energy from the quasar itself in the form of radiation and gas outflows, may heat and expel gas from the dark matter halos in the LSS, hampering further star formation and galaxy assembly (e.g. Costa et al. 2014). This "negative feedback" may in fact complicate the detection of these early structures, especially within a few hundreds kpc from the quasar. To date, empirical evidence of overdensities around early SMBHs remains elusive. The attempts to directly measure galaxy overdensities have started since the discovery of high-z quasars, mainly by selecting Lyman Break Galaxy (LBG) and Lyman Alpha Emitter (LAE) candidates at the QSO redshift, but the results have not been con-

⋆ e-mail: marco.mignoli@inaf.it

clusive (see e.g. Mazzucchelli et al. 2017). Recently, Ota et al. (2018) reported an example of a candidate LSS extending for ∼4×8 pMpc^2 (i.e. 12′×24′) in the vicinity of a z=6.6 QSO. Their Subaru Suprime-Cam narrow and broadband photometric observations select both LBG and LAE candidates: the low density of LAEs within 3 pMpc from the QSO may hint at negative feedback acting preferentially on low-mass galaxies hosted by small halos.

Further insight is now coming from ALMA: [CII] observations of a sample of 25 QSOs with $M_{BH} \gtrsim 3 \times 10^8\ M_\odot$ at z>5.94 revealed that a significant fraction of them (16%) are paired to a close (within ∼100 kpc) companion galaxy that is rapidly forming stars (Decarli et al. 2017). This suggests that early SMBH fueling and galaxy assembly may be favored by galaxy interactions on very small scales, but the presence of any significant structure on larger scales has still to be firmly established (Habouzit et al. 2019).

With the aim of obtaining the first observational confirmation of an LSS around a super-massive black hole in the first billion years of the Universe, we started an intensive observational campaign of the field around the bright QSO SDSS J1030+0524 (z=6.308, $M_{\rm BH}$=1.4×10$^9 M_\odot$; Kurk et al. 2007), where promising evidence for a high-z LSS was reported (see Section 2).

Throughout this Letter we adopt a concordance cosmology with H_0 = 70 km s^{-1} Mpc^{-1}, Ω_m= 0.3, and Ω_Λ = 0.7, in agreement with the values measured by the Planck Collaboration XIII (2016). This gives a scale of 5.55 kpc/arcsec at z=6.308. All magnitudes are total magnitudes and quoted in the AB system.

2. SDSS J1030+0524: an over-dense QSO field

Among the ≈300 QSOs discovered so far at z>5.7 (Bañados et al. 2016), SDSS J1030+0524 (hereafter J1030) is hosted in one of the most convincing large-scale galaxy overdensities. Deep imaging with the 3′×3′Advanced Camera for Surveys (ACS) on the Hubble Space Telescope (HST) revealed a ∼3σ overdensity of i-band dropouts within ∼0.5 projected pMpc from the QSO (Stiavelli et al. 2005; Kim et al. 2009). Among all of the z∼6 QSO fields observed with HST by Kim et al. (2009), J1030 was found to be the most overdense.

In the sample of four luminous z∼6 QSOs observed with the Large Binocular Camera (LBC) at the Large Binocular Telescope (LBT) by Morselli et al. (2014), J1030 was found again to feature the highest density of i-band dropouts (with density contrast $\delta = \rho/\bar{\rho} - 1 = 2$, at S/N=3.3; ρ and $\bar{\rho}$ are the measured and average, background, source density, respectively), hence reinforcing the result found on (8×) smaller scales by Stiavelli et al. (2005). In 2016, we obtained deep ($Y_{\rm AB}$=24.5, $J_{\rm AB}$=24) near-IR imaging of the J1030 field with the Wide-field InfraRed Camera at the Canada France Hawaii Telescope[1]. Using these new observations, together with archival data from the *Spitzer* Infrared Array Camera (IRAC), Balmaverde et al. (2017) pushed the selection of z∼6 galaxy candidates to fainter fluxes, measured photometric redshifts, and improved the rejection of contaminants. This analysis allowed the selection of 21 robust z∼6 candidates down to $z_{\rm AB}$∼25.7, reinforcing the significance of the LSS overdensity, now with δ=2.4, at S/N=4.0. Similarly to what observed by HST/ACS on smaller scales, a strong asymmetry in the spatial distribution of these brighter dropouts was found on larger scales (See Fig. 1).

[1] See http://j1030-field.oas.inaf.it/ for a summary of all data-sets available in the field.

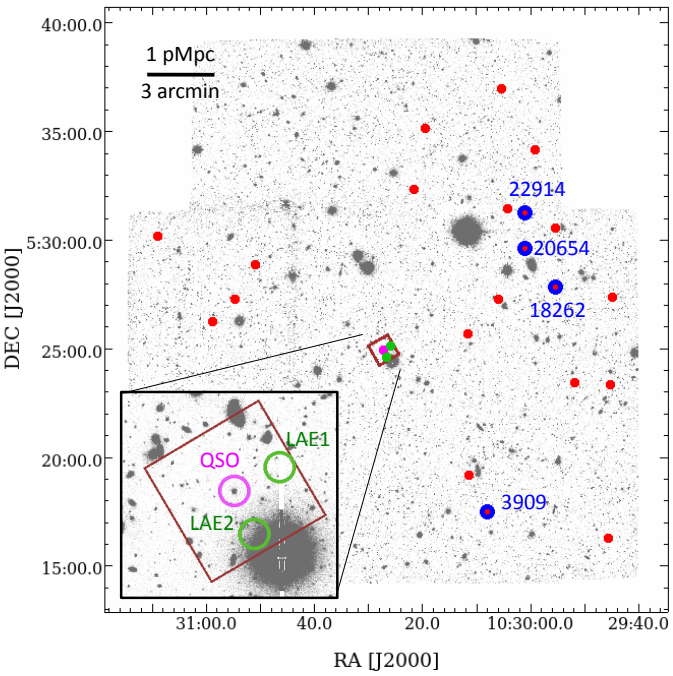

Fig. 1: Sky distribution of the LBG sample (red dots) overplotted to the LBT/LBC z-band image of the field. The spectroscopically confirmed members of the LSS at the QSO redshift are marked in blue and labeled with their ID. The position of the two LAEs in the LSS discovered by MUSE is marked by green points. The MUSE field of view (FoV) is shown as a brown square. The position of the QSO is shown in magenta. The inset shows a zoom on the sky region around the MUSE field.

3. Spectroscopic campaign and UV properties of the galaxy members

We started a systematic program of spectroscopic follow-up of the z∼6 LBG candidates selected in Balmaverde et al. (2017), to precisely measure their redshifts and to verify if they are actually located in the vicinity of the central QSO. The campaign used several multi-object spectrographs (MOS): the DEep Imaging Multi-Object Spectrograph (DEIMOS) on the 10-m Keck II telescope (Faber et al. 2003), the FOcal Reducer and Spectrograph (FORS2, Appenzeller et al. 1998) and the Multi Unit Spectroscopic Explorer (MUSE, Bacon et al. 2010), both mounted on the Very Large Telescopes (VLTs) at ESO, and, finally, the Multi-Object Dual Spectrograph (MODS, Pogge et al. 2010) at the LBT. Details on the observing runs and on the analysis of the spectroscopic data are presented in Appendix A.

In summary, we observed 12 out of the 21 LBGs selected by Balmaverde et al. (2017): nine of them resulted in bona-fide high-redshift (z>5.7) galaxies, while the low spectral quality and absence of significant spectral features prevented any redshift determination for the remaining three. In the archival VLT/MUSE cube centered on the QSO, we further detected four LAEs with z>5.7: none of them was selected by Balmaverde et al. (2017) because they are fainter than the magnitude limits of the LBT photometric data. We note that the distinction between LBGs and LAEs adopted for our targets refers essentially to the selection method, since LBGs may also display Lyα emission.

We considered the six galaxies with $|z - z_{QSO}| < 0.1$ (four LBGs and two LAEs, see Table 1 and Fig. 1) as part of the LSS around the QSO (see Section 4 for the exact procedure adopted

to identify LSS members). The galaxies' spectra are shown in Fig. 2 (for three LBGs; the spectrum of LBG #22914 has been already published in Decarli et al. 2019) and Fig. 3 (for the two LAEs). The spectral and photometric properties of the six galaxies are presented in Table 1. In Fig. 4 we compare their rest-frame Lyα equivalent widths (EW) with absolute UV magnitudes (M_{UV}). Here M_{UV} is the monochromatic magnitude at 1350Å, which, at $z\approx6.3$, roughly corresponds to the effective wavelength of the LBC z-band magnitude from which it was obtained. Although the number of galaxies is limited, we observe the same trend reported in numerous previous studies of high-z field galaxies: UV-bright LBGs shows limited Lyα EWs ($\ll$20Å), while the fainter LAEs exhibit larger EWs. Our objects almost overlap with the larger sample of high-z ($5.4<z<6.5$) galaxies collected and analyzed by De Barros et al. (2017). A detailed comparison would require further spectroscopic identification of galaxies around J1030. Nonetheless, this preliminary analysis shows that the UV spectral properties of galaxies in this LSS do not differ significantly from those of field galaxies at high redshift.

4. Redshift distribution and significance of the overdensity

The redshift distribution of all spectroscopically confirmed LBGs and LAEs at $z\sim6$ is shown in Fig. 5 (top and bottom panel, respectively). The distributions are shown in redshift bins of Δz=0.1 (orange histogram), as well as in finer, Δz=0.005, bins (red histogram). To isolate potential peaks in the redshift distribution avoiding binning dependencies, we used a procedure similar to that described in Gilli et al. (2003). We smoothed the unbinned redshift distribution using a Gaussian with σ_z=0.1 (red dashed line). We recall that, at $z\sim6$, a separation of 0.1 in redshift space corresponds to a separation of about 5 pMpc (assuming negligible peculiar velocities). This physical scale corresponds to the maximum projected separation between the QSO and the candidate companion galaxies in the LBT/LBC image, and is consistent with the observed transverse dimension of other $z\sim6$ LSSs (e.g. Ota et al. 2018). A clear peak at $z\simeq6.275$ is observed in both the LBGs and LAEs smoothed distributions (red dashed curves in Fig. 5). We note that the QSO redshift is included in the determination of the peak position of both redshift distributions (as it would have been selected in both samples), but not in the computation of the structure significance described below. We also note that, for the LBGs, the observed peak falls at a significantly higher redshift than that expected by the i-band dropout selection technique (Bouwens et al. 2003, 2007; Ono et al. 2018), suggesting that an LSS is indeed present at $z\sim6.3$.

Once the peak position is determined, we counted all galaxies within $\Delta z\pm0.1$, i.e. within 5 pMpc, from the peak redshift (brown dotted lines in Fig. 5). The four LBGs and two LAEs of Table 1 fall in this interval. In order to estimate the expected background of LBGs in that interval we used the selection function derived in deep HST fields by Bouwens et al. (2007) for i-band dropouts selected by means of color criteria similar to ours (e.g. i-z>1.3 as the main selection criterion). Two other "background" curves are shown in Fig. 5: one for faint i-band dropouts selected in HST/ACS GTO fields (Bouwens et al. 2003) and one for i-band dropouts as bright as ours, selected as part of the HSC GOLDRUSH project (Ono et al. 2018). The selection criterion in both Bouwens et al. (2003) and Ono et al. (2018) is i-z>1.5. All these background curves have been normalized to 21, i.e. to the total number of candidate LBGs selected by Balmaverde et al. (2017). Despite the differences produced by the different color cuts adopted, they all show that the maximum efficiency of i-band dropout selection is between $z\sim5.7$ and 6. By using the Bouwens et al. (2007) distribution, we derive a probability of 0.12 that one galaxy falls in the considered redshift interval. We note that the adopted background curve has the highest efficiency at z=6.3 among the three curves. Therefore, our choice is the most conservative. Based on the binomial distribution, the probability that 4 (or more) out of 9 spectroscopically confirmed LBGs fall in the selected redshift interval, when the expectation of observing one is 0.12, is P_{LBG}=0.0159.

We adopted a similar procedure to estimate the binomial probability that two out of four MUSE LAEs fall in the same redshift interval. To estimate a background source distribution, we considered the spectroscopic catalog obtained from the 3′×3′ MUSE observation of the Hubble Ultra Deep Field (HUDF, Beckwith et al. 2006) consisting of 9 pointings of 10 hr each (Bacon et al. 2017; Inami et al. 2017). We heavily smoothed

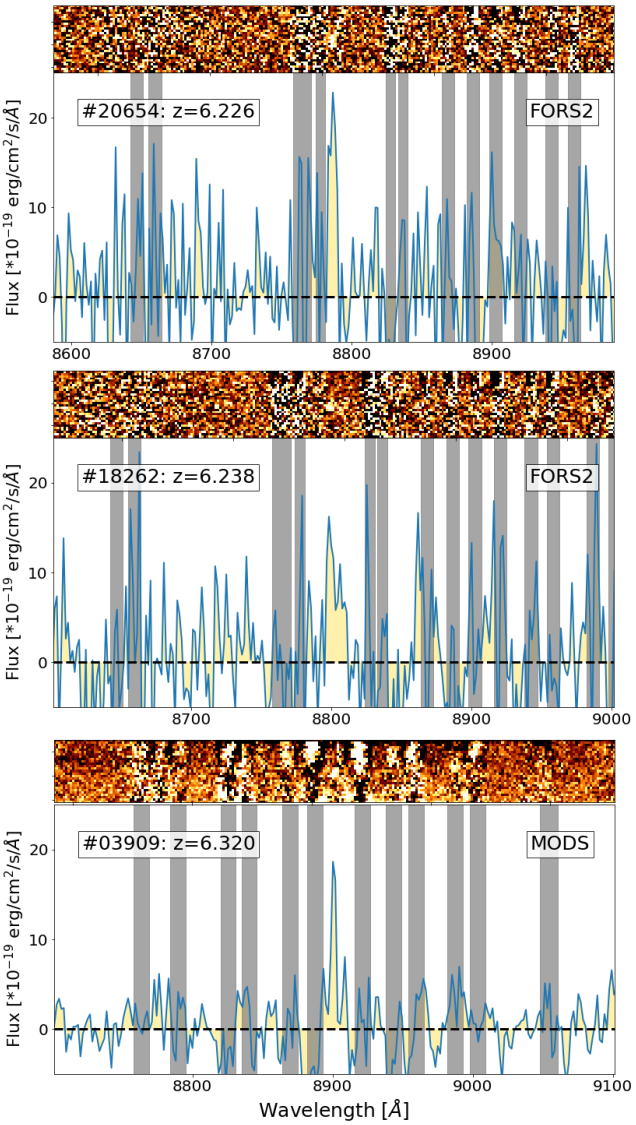

Fig. 2: Optical spectra of three LBGs in the LSS with redshift measured from the peak of Lyα line (see Table 1). In each panel the top row shows the 2D-spectrum, while at the bottom the 1D-spectrum is displayed with gray bands highlighting the spectral regions inaccessible due to the strong sky line residuals.

Table 1: Identified LBGs & LAEs

ID	mag z-band	M_{UV}	logSFR	redshift	Instrument	Lyα Flux	Lyα EW
(1)	(2)	(3)	(4)			(5)	(6)
22914	25.45±0.22	-21.61	1.70	6.319±0.001	DEIMOS	<3[a]	<5
20654	25.27±0.17	-21.77	1.97	6.226±0.002	FORS2	8.5±0.2	14
18262	25.70±0.20	-21.34	1.32	6.238±0.004	FORS2	5.3±0.3	13
03909	25.55±0.19	-21.51	1.55	6.320±0.003	MODS	5.0±0.3	16
LAE1	≈27[b]	-20.03	0.40	6.219±0.002	MUSE	3.7±0.2	27
LAE2	>26.5[c]	>-20.5	<0.6	6.355±0.001	MUSE	3.0±0.2	>11

Notes. (1) Source ID; (2) AB total magnitude. IDs and mags are from Balmaverde et al. (2017), except for the two MUSE-detected LAEs and ID22914 (see Appendix A); (3) monochromatic magnitude at 1350Å (4) logarithm of the Star Formation Rate in units of $M_\odot$/yr, computed from the UV luminosity adopting the Kennicutt (1998) calibration; (5) line fluxes in units of 10^{-18} erg/s/cm^2; (6) rest-frame equivalent widths in Å. [a] 3-σ upper limit estimated from the continuum S/N; [b] synthetic magnitude estimated by convolving the spectrum with the LBC z-band filter response; [c] LAE2 is not detected in the continuum in the MUSE spectrum and is undetected both in the LBT/LBC and HST photometry, so we adopted the 5σ magnitude limit measured in the ACS F850LP image.

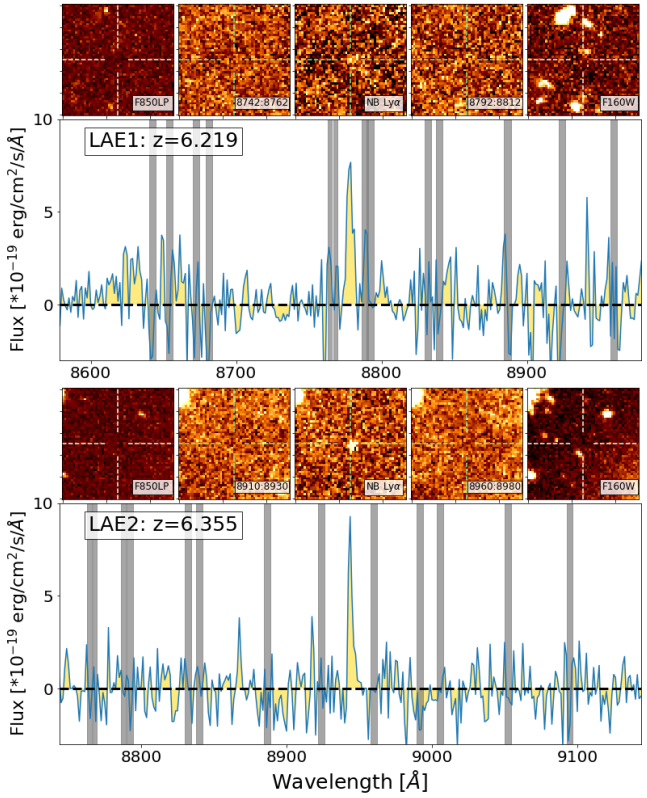

Fig. 3: MUSE spectra of the two LAEs in the LSS (see Table 1) are displayed in two panels. In each panel the top row shows, from left to right, the HST/ACS F850LP image, three MUSE reconstructed narrow-band images (20Å-wide), and the HST/Wide Field Camera 3 (WFC3) F160W image. The images are 10″ wide and the source position is indicated by cross-hairs. In the bottom row, the extracted 1D-spectrum is shown in a 400Å-wide interval around the Lyα line, with noisy regions in the MUSE cube affected by the sky line subtraction highlighted by gray bands.

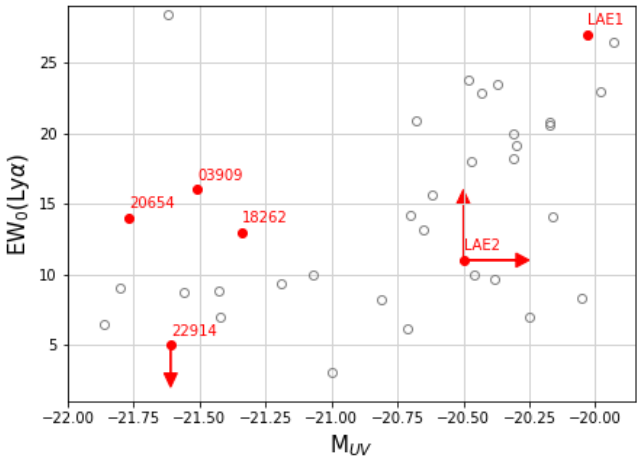

Fig. 4: EW(Lyα) vs. M_{UV} for the six LSS-member galaxies of Table 1 (red filled circle). For comparison we also plot the same properties from a large sample of high-z galaxies, presented by De Barros et al. (2017) (gray empty circles).

the MUSE HUDF redshift distribution using a Gaussian with σ_z=0.5 and then re-normalized it to the average number of galaxies expected in a single pointing of the HUDF (gray line in the bottom panel of Fig. 5). Based on this procedure, we would expect a total of 9 LAEs at z>5.2 in our field, which gives a probability of observing one in the considered redshift interval equal to 0.062. We note that if anything, this procedure probably overestimates the average galaxy background density because the HUDF observations are deeper than those in the J1030 field and then likely return a redshift distribution skewed towards slightly higher redshifts. Hence, the derived significance may again be regarded as conservative. Based on the binomial distribution, the probability that 2 (or more) out of 4 spectroscopically confirmed LAEs fall in the considered redshift interval, when the probability of observing one is 0.062, is $P_{\rm LAE}$=0.0212.

By simply combining the two probabilities computed above, we finally estimate that the structure is detected at the $1-P_{\rm LBG}\times P_{\rm LAE}$ = 0.9997 confidence level, which corresponds to 3.5σ in Gaussian statistics. We double checked these numbers by running Monte Carlo simulations drawing 9 LBGs and 4 LAEs from the redshift probability distributions described above. We run 10^5 realizations and checked how many times four or more LBGs and two or more LAEs fall in the considered redshift interval. The probability values obtained by the simulations are identical to those obtained with the binomial statistics.

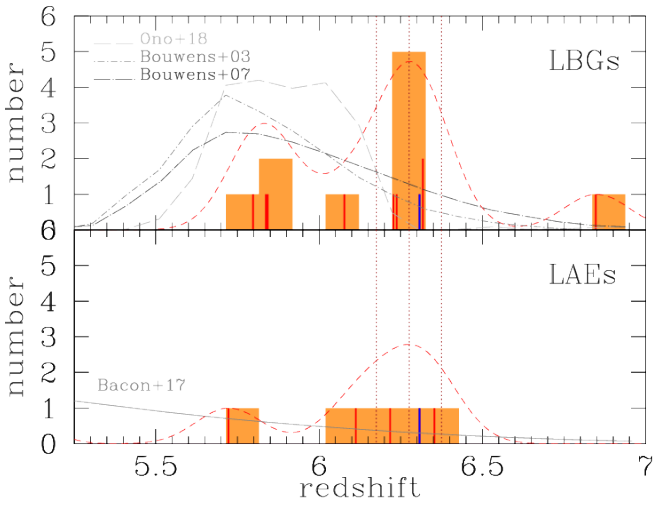

Fig. 5: *Upper panel:* Redshift distribution of all spectroscopically confirmed LBGs at z~6 in the J1030 field. The orange and red histogram have bins of Δz=0.1 and 0.005, respectively. The dashed red curve has been obtained by smoothing the unbinned distribution with a Gaussian with σ_z=0.1 (arbitrarily normalized). The redshift peak and $\Delta z \pm 0.1$ interval used to estimate the structure significance are shown by the brown vertical dotted lines. The three gray lines show the selection function of i-band dropout samples in the literature (see labels) with selection criteria similar to ours. *Lower Panel:* Same as in the upper panel but for LAEs selected with MUSE. The gray curve is obtained by heavily smoothing the redshift distribution of LAEs observed with MUSE in the HUDF (Bacon et al. 2017). The QSO redshift (marked in blue) is included in the orange histograms in both panels.

5. Discussion and Conclusions

5.1. Robustness of the structure detection

We show here that the 3.5σ level derived in the previous section is a robust lower limit to the LSS detection significance.

First we note that there is no bias in our observations towards sources at z~6.3. From Fig. 2 it is evident that a significant fraction of the red spectral range is blinded by the noise produced by the subtraction of the strong night-sky lines, making the detection of faint Lyα lines highly inefficient. The distribution of sky lines is nonetheless rather uniform across the z=5-7 redshift range. As the probability of successfully measuring the redshift of a source inside or outside the structure is the same, we then observe a number of redshifts in and out the structure that have been likely depressed by the same factor. Accounting for this effect would increase the statistical significance of the LSS detection. Also, we did not fine tune the smoothing length and width of the structure interval to maximize the signal. As an example, repeating the computations using $\delta_z \sim 0.08$ around the peak redshift, would increase the significance to 3.7σ. In our significance computations we conservatively never included the QSO. However, the QSO is part of the structure and it would have been selected in both the LBG and LAE samples discussed above. If we include it in the LBG sample and compute the binomial probability that 5 out of 10 sources extracted from the same probability distribution adopted above fall in the considered redshift range, we obtain $P_{\rm LBG}$=0.0037. When combined with $P_{\rm LAE}$ computed above this gives a joint significance of 3.8σ. Finally, in our computations we considered among the possible reference background curves, those that are more skewed towards the highest redshifts, i.e. those returning the highest background probability of observing a galaxy around z~6.3. This choice is very conservative. For instance, by adopting the redshift distribution of i-band dropouts of Ono et al. (2018), which shows a sharp drop beyond z=6, we would estimate a joint significance of $> 4\sigma$.

5.2. Overdensity level

At present, the number of LBGs that have been spectroscopically identified as part of the LSS around the QSO is $n = 4$, whereas one would expect an average of $\bar{n} \sim 2$ assuming the Bouwens et al. (2007) redshift probability distribution normalized to 21, i.e. the total number of LBGs in the J1030 field (Balmaverde et al. 2017). This corresponds to a lower limit to the measured level of the spectroscopic overdensity of $\delta = n/\bar{n} - 1 \geq 1$ ($\geq$1.5 if the QSO is added), as subsequent successful identifications of LBGs at z~6.3 from the Balmaverde et al. (2017) sample will simply increase n. Also, the total number of LBGs in the field is likely enhanced by the presence of the LSS and the adopted value for $\bar{n}$ presumably overestimates the true average density. Consequently, the lower limit to δ estimated above is conservative (based on similar arguments, we derive a lower limit to the LAE overdensity of $\delta_{\rm LAE} \geq 2.3$). We note that the estimated overdensity level is measured over a remarkably large volume of ~780 pMpc^3, and is consistent, within the statistical errors, with what was measured through imaging by Balmaverde et al. (2017).

Based on the observed overdensity, we provide a rough estimate of the clustering level of early galaxies and QSOs that is required to explain it. To this aim, the expected overdensity level can be obtained by integrating the LBG-QSO cross-correlation function (assumed here to be a power-law $\xi(r) = (r/{\rm r}_{0,\rm QG})^{-\gamma}$ with cross-correlation length $r_{0,\rm QG}$) over the considered volume. For simplicity, we use for this computation a sphere of radius r_s=5.7 pMpc around the QSO, which contains all the LBGs in the LSS, and has the same volume considered in the previous sections (780 pMpc^3, i.e. a cylinder of both radius and half-length 5 pMpc). This gives $\delta(< r_s) = 3\xi(r_s)/(3-\gamma)$. An overdensity of $\delta >$1.0−1.5, as observed e.g. for our LBGs, would require $r_{0,\rm QG} > 24-29$ Mpc comoving (cMpc) for γ=2. Assuming that the auto-correlation functions of QSOs and galaxies are both power-laws with the same slope, the relation $r_{0,\rm QG}=(r_{0,\rm QQ}\times r_{0,\rm GG})^{1/2}$ holds, where $r_{0,\rm QQ}$ and $r_{0,\rm GG}$ are the auto-correlation lengths of QSOs and galaxies, respectively. As $r_{0,\rm GG} \approx 20-30$ cMpc for galaxies at $z\sim 6$ with M_{UV} and star formation rate (SFR) similar to ours (Khostovan et al. 2019), we estimate that $r_{0,\rm QQ}$ is at least ~20 cMpc. Such a large correlation length at z~6 in turn suggests that J1030 is hosted by a dark matter halo with mass $M_{\rm h} > 10^{12}\ M_\odot$ (Harikane et al. 2018; Khostovan et al. 2019).

5.3. Environment of early black holes: future prospects

Although simulations suggest that SMBHs in the early Universe should reside on average in the most massive ($10^{12-13}\ M_\odot$) dark matter halos formed at that time, a large variance in the galaxy number counts around them is nonetheless expected, and some SMBHs may not even show enhanced counts in their neighborhoods (Habouzit et al. 2019). The expected variance is even larger when feedback effects are considered, either from the QSO itself or from strong stellar winds in the companion galaxies (Costa et al. 2014). Such feedback effects may suppress star

formation, and hence decrease the luminosity and stellar mass of the galaxy members within scales of 1-2 pMpc, which would then fall below the sensitivity of most observations of high-z QSO fields.

To obtain a reasonable census of the environment of high-z QSOs, explorations of deep-and-wide areas around several such systems is needed. Our approach based on LBT/LBC observations is along these lines (see also Ota et al. 2018, for deep-and-wide observations with Subaru/Suprime-Cam). Expensive follow-up observations with optical spectrographs at 8-10m class telescopes are needed to secure redshifts of the relatively luminous LBG candidates selected over wide areas, as these may have weak Lyα lines. As shown in Fig. 2, such observations are complicated by the presence of strong sky lines. High-z LAEs, on the other hand, can be nowadays efficiently selected with MUSE down to very faint fluxes. The main limitation with such an approach is the small FoV of MUSE, which requires a large number of pointings. The analysis presented in this paper shows that obtaining a robust estimate of the galaxy density around early QSOs is an extremely time-consuming process, even for a single system.

A complementary approach to obtain accurate redshifts is searching for the [CII]158 μm or the [OIII]88 μm line in spectroscopic observations at (sub-)mm frequencies (e.g. Decarli et al. 2017; Hashimoto et al. 2019; Harikane et al. 2020). This approach is particularly promising as it allows for a redshift estimate in those LBG candidates with absent or weak Lyα (Decarli et al. 2019), or falling in redshift windows covered by sky lines (see Fig.2). Also, it allows for the discovery of dusty companion galaxies that cannot be selected at any other wavelength (Decarli et al. 2017). ALMA observations are then an extremely promising tool to identify members of LSSs around z~6 QSOs. In particular, for the J1030 field, such observations may increase the statistical significance of the overdensity reported in this paper and, importantly, deliver a sizeable sample of confirmed members that we can use to identify common trends and/or systematic differences in the physical properties of LSS and field galaxies at z~6.

Acknowledgements. We thank the referee for careful reading and detailed report that improved the quality of the manuscript. We acknowledge funding from the INAF main-stream (1.05.01.86.31) and from the agreement ASI-INAF n. 2017-14-H.O. This work is based on ESO program 0102.A-0263(A), on observations obtained at the W. M. Keck Observatory, and on data acquired using the Large Binocular Telescope (ID 2017/2018 #18).

References

Appenzeller, I., Fricke, K., Fürtig, W., et al. 1998, Msngr, 94, 1
Bacon, R., Accardo, M., Adjali, L., et al. 2010, Proc. SPIE, 7735, 8
Bacon, R., Conseil, S., Mary, D., et al. 2017, A&A, 608A, 1
Balmaverde, B., Gilli, R., Mignoli, M., et al. 2017, A&A, 606A, 23
Bañados, E., Venemans, B.P., Decarli, R., et al. 2016, ApJS, 227, 11
Barai, P., Gallerani, S., Pallottini, A., et al. 2018, MNRAS, 473, 4003
Beckwith, S.V.W., Stiavelli, M., Koekemoer, A.M., et al. 2006, AJ, 132, 1729
Bouwens, R.J., Illingworth, G.D., Rosati, P., et al. 2003, ApJ, 595, 589
Bouwens, R.J., Illingworth, G.D., Franx, M., et al. 2007, ApJ, 670, 928
Costa, T., Sijacki, D., & Haehnelt, M.G. 2014, MNRAS, 444, 2355
De Barros, S., Pentericci, L., Vanzella, E., et al. 2017, A&A, 608A, 123
Decarli, R., Walter, F., Venemans, B. P., et al. 2017, Nature, 545, 457
Decarli, R., Mignoli, M., Gilli, R., et al. 2019, A&A, 631L, 10
Faber, S. M., Phillips, A. C., Kibrick, R. I., et al. 2003, Proc. SPIE, 4841, 1657
Gilli, R., Cimatti, A., Daddi, E., et al. 2003, ApJ, 592, 721
Gilli, R., Mignoli, M., Peca, A., et al. 2019, A&A, 632A, 26
Habouzit, M., Volonteri, M., Somerville, R.S., et al. 2019, MNRAS, 489, 1206
Harikane, Y., Ouchi, M., Ono, Y., et al. 2018, PASJ, 70S, 11
Harikane, Y., Ouchi, M., Inoue, A.K., et al. 2020, ApJ, 896, 93
Hashimoto, T., Inoue, A.K., Tamura, Y., et al. 2019, PASJ, 71, 71
Inami, H., Bacon, R., Brinchmann, J., et al. 2017, A&A, 608A, 2
Khostovan, A.A., Sobral, D., Mobasher, B., et al. 2019, MNRAS, 489, 555
Kennicutt, R. 1998, ARA&A, 36, 189
Kim, S., Stiavelli, M., Trenti, M., et al. 2009, ApJ, 695, 809
Kreckel, K., Groves, B., Bigiel, F., et al. 2017, ApJ, 834, 174
Kurk, J.D., Walter, F., Fan, X., et al. 2007, ApJ, 669, 32
Mazzucchelli, C., Bañados, E., Decarli, R., et al. 2017, ApJ, 834, 83
Mignoli, M., Zamorani, G., Scodeggio, M., et al. 2009, A&A, 493, 39
Morselli, L., Mignoli, M., Gilli, R., et al. 2014, A&A, 568A, 1
Nanni, R., Gilli, R., Vignali, C., et al. 2020, A&A, 637A, 52
Ono, Y., Ouchi, M., Harikane, Y., et al. 2018, PASJ, 70S, 10
Ota, K., Venemans, B. P., Taniguchi, Y., et al. 2018, ApJ, 856, 109
Overzier, R.A., Guo, Q., Kauffmann, G., et al. 2009, MNRAS, 394, 577
Planck Collaboration, Ade, P.A.R., Aghanim, N., et al. 2016, A&A, 594A, 13
Pogge R. W., Atwood B., Brewer D. F., et al. 2010, Proc. SPIE, 7735, 9
Sijacki, D., Springel, V., Haehnelt, M.G. 2009, MNRAS, 400, 100
Stiavelli, M., Djorgovski, S.G., Pavlovsky, C., et al. 2005, ApJ, 622L, 1
Urrutia, T., Wisotzki, L., Kerutt, J., et al. 2019, A&A, 624A, 141
Wise, J.H., Regan, J.A., O'Shea, B.W., et al. 2019, Nature, 566, 85

Appendix A: Observing runs and spectral analysis

Appendix A.1: DEIMOS observations

We observed our $z\sim6$ candidates with DEIMOS on Feb 27, 2017. We used the 830 lines mm^{-1} grating, and the OG550 order cut filter with the central wavelength of 8500Å, to efficiently cover the red spectral range >7000Å. Because of bad weather, we observed only one of the two designed masks, and the exposure time was reduced to four hours instead of the planned six. Nine candidate high-z galaxies from Balmaverde et al. (2017) were included in the observed slitmask: three of them were confirmed to be genuine high-redshift (z>5.7) LBGs, other two showed very faint (S/N$\lesssim$2) features compatible with a redshift larger than six (but one of the two unsecure identifications was LBG #20654, subsequently confirmed by deeper FORS2 observations), while the remaining four were too noisy or even undetected. We also included in the masks an LBG candidate, #22914, that was not part of the original sample of Balmaverde et al. (2017), but was subsequently included after revision of the photometric errors. We measured for LBG #22914 a redshift of z=6.319 based on a clear Lyman break in the spectrum. The redshift was later confirmed by the detection of a [CII]158 μm line in the NOEMA mm-band spectrum (Decarli et al. 2019, the DEIMOS spectrum is shown in their Fig. 1).

Appendix A.2: FORS2 observations

During the ESO observing period P102 we were granted VLT/FORS2 observations to obtain spectra of the $z\sim6$ LBG candidates with three 10 hours-long masks. In the first months of 2019 around one third of the project was completed in service mode. We used FORS2 equipped with MIT red-optimized CCD and adopted grism 600Z+23 to observe the wavelength range 7000−11000Å covering the redshifted Lyα position for z>5.15. The only and partially (80%) completed mask included 8 primary targets: four of them have been spectroscopically confirmed as high-z LBGs and two of them reside in the $z\simeq6.3$ structure. The two upper panels of Fig. 2 show portions of the 2-D and 1-D spectra covering the only spectral feature visible in the full observed spectral range: the well detected emission line is identified as Lyα. We can confidently rule out other possible line identifications and redshift solutions. The low-z solutions, with the emission line associated with either Hα, [O III]λ5007, or Hβ, are discarded due to the lack of the expected nearby lines and because the broadband colors of these solutions are generally inconsistent with the *i*-dropout selection. The most plausible alternative identification is [O II]λ3727 at $z\simeq1.4$, but this emission line would be resolved into a doublet at our spectral resolution, which is not observed. In the LBG #20654 spectrum an unresolved emission line is detected with a formal S/N=9 at the observed wavelength of 8787Å, placing this objects at z=6.226. The line is also detected, albeit with much lower significance, in a DEIMOS spectrum, further confirming its authenticity. The FORS2 spectrum of LBG #18262 shows a slightly resolved emission line, detected with S/N=8 at the observed wavelength of 8801Å. The line is undoubtedly asymmetric with a red wing, a typical shape of high-redshift Lyα emission lines, and yields a redshift of z=6.238 for this source.

Table A.1: Table of spectroscopic observations

Telescope	Instrument	Date	Exp.Time	Spectral Range (1)
VLT	MUSE	2015-2016	23040s	4750−9350 Å
Keck	DEIMOS	Feb 2017	14400s	≈7000−10500 Å
VLT	FORS2	Jan-Mar 2019	29055s	≈7000−11000 Å
LBT	MODS	2018-2019	14400s	≈5400−10000 Å

Notes. (1) The spectral ranges reported for the slit spectrographs are indicative, as they depend on the geometrical position of the slit within the mask used for the MOS observation.

Appendix A.3: MODS observations

In 2017 we were granted an INAF-LBT Strategic Program[2] to identify the X-ray sources detected with a ∼500 ks Chandra exposure in the J1030 field (Nanni et al. 2020). As part of this large (52 hours) optical/NIR program, we observed in 2018 and 2019 a total of 9 MODS masks mainly dedicated to spectroscopically follow up X-ray sources. The observations were obtained in dichroic mode to obtain blue (with the G400L grating) and red (with G670L grating) spectra simultaneously on the blue and red spectrograph channels. Since the density of the X-ray counterparts was well matched with the number of slits that can be placed in each mask, only few $z\sim6$ LBG candidates were included as fillers in this program. Therefore, and also because of the limited exposure time per mask (4hr) only one LBG was identified through MODS observations. The MODS spectrum of LBG #03909 (bottom panel of Fig.2) shows an unresolved emission line detected with S/N=6 at the observed wavelength of 8901Å, placing this objects at z=6.320. The same considerations given above for the FORS2 observations exclude emission lines other than Lyα.

Appendix A.4: Archival MUSE observations

The J1030 field was observed with MUSE in April 2015 and then again in January 2016 under the ESO program ID 095.A-0714 (PI Karman). MUSE is an integral field spectrograph with a one arcmin^2 field-of-view and a spatial sampling of 0.2×0.2 arcsec^2, covering the wavelength range 4750−9350 Å with a spectral bin of 1.25 Å pixel^{-1}. The data reduction and analysis of the archival 6.4hr MUSE data are presented in Gilli et al. (2019). In brief, we measured a redshift for 102 objects (16 of them at z>4) in the square arcmin region around the central QSO, a region that did not include any of the LBG candidates selected by Balmaverde et al. (2017). In spite of that, MUSE observations revealed four Lyman Alpha Emitters (LAEs) at z>5.7, with two of them at $z\approx6.3$. The MUSE observations of LAE1 is shown in the top panel of Fig.3. In the 1-D spectrum an unresolved emission line is detected with S/N=9 at the observed wavelength of 8778Å, placing this objects at z=6.219. The MUSE spectrum of LAE2 shows a strong unresolved emission line detected with S/N=10 at the observed wavelength of 8944Å. The line is asymmetric with a red wing and yields a redshift of z=6.355. The source is not detected in the continuum, nor in the HST F850LP and F160W filters. The non-detections of MUSE-selected LAEs in medium-deep HST images is not uncommon, as shown by the MUSE-Wide Survey, where 55% of z>2.9 LAEs are undetected in deep CANDELS photometric catalogs (Urrutia et al. 2019).

[2] ID 2017/2018 #18 (P.I. R. Gilli).

Appendix A.5: Spectra calibration and analysis

The spectra of the LBGs targeted with MOS instruments were flux-calibrated using observations of spectro-photometric standard stars obtained during the observing runs. The spectra were further calibrated using the z-band magnitudes presented in Table 1, by integrating the spectra over the known LBC filter bandpasses. Since all the observations were performed in good seeing conditions ($\lesssim 1''$) and with slit-width of $1-1.2''$, the relatively small corrections amount up to $\approx$50%. The absolute flux calibration of the MUSE data is very good (Kreckel et al. 2017) and the absence of flux losses is further demonstrated by the excellent agreement between the optical magnitudes obtained from our LBC broad-band photometry and the synthetic magnitudes estimated from MUSE spectra. The redshift of all the galaxies presented for the first time in this paper has been measured from position of the Lyα emission peak. The redshift value is consistent, within the errors, with that obtained from the Gaussian fit of the line, apart from the two objects (LBG #18262 and LAE2) in which Lyα has an asymmetrical profile and the peak position is known to provide a more correct redshift estimation. The fluxes of the Lyα emission of Table 1 were measured by integrating the flux over the line profile. The upper limits of flux and equivalent width of the Lyα line in #22914 were estimated from the continuum S/N and the spectral resolution following the recipe of Mignoli et al. (2009). LAE1 is not detected in the LBT/LBC nor in the HST photometry, but a very low S/N continuum redward of the emission line is marginally detected in the MUSE spectrum, from which we derived a synthetic magnitude $z_{\rm AB}$ of $\approx$27 by integrating the continuum convolved with the LBC z-band filter response. This value is compatible with the non-detection of the source in the HST/ACS F850LP image (leftmost box in the upper row of the LAE1 panel in Fig. 3; $\rm AB_{5\sigma} \sim 26.5$). LAE2 is not detected in the continuum neither in the MUSE spectrum nor in the HST photometry, then we used the 5-σ magnitude limit of 26.5 estimated from the HST/ACS F850LP image to constrain the UV continuum flux. This upper limit in the continuum yields the lower limit of the Lyα equivalent width quoted in Table 1.